Photochemistry and Photobiology, 2017, 93: 733–740

Time-Resolved Energetics of Photoprocesses in Prokaryotic Phytochrome-Related Photoreceptors†

Aba Losi*[1], Hernán R. Bonomi[2], Norbert Michael[3], Kun Tang[4,5‡] and Kai-Hong Zhao[4]

[1]Department of Physics and Earth Science, University of Parma, Parma, Italy
[2]Immunology and Molecular Microbiology Laboratory, Fundación Instituto Leloir, Buenos Aires, Argentina
[3]Institut für Chemie, Technische Universität Berlin, Berlin, Germany
[4]State Key Laboratory of Agricultural Microbiology, Huazhong Agricultural University, Wuhan, China
[5]Max Planck Institute for Chemical Energy Conversion, Mülheim an der Ruhr, Germany

Received 30 October 2016, accepted 7 December 2016, DOI: 10.1111/php.12728

ABSTRACT

Time-resolved photoacoustics (PA) is uniquely able to explore the energy landscape of photoactive proteins and concomitantly detects light-induced volumetric changes (ΔV) accompanying the formation and decay of transient species in a time window between ca. 20 ns and 5 μs. Here, we report PA measurements on diverse photochromic bilin-binding photoreceptors of prokaryotic origin: (1) the chromophore-binding GAF3 domain of the red (R)/green (G) switching cyanobacteriochrome 1393 (*Slr*1393g3) from *Synechocystis*; (2) the red/far red (R/FR) *Synechocystis* Cph1 phytochrome; (3) full-length and truncated constructs of *Xanthomonas campestris* bacteriophytochrome (*Xcc*BphP), absorbing up to the NIR spectral region. In almost all cases, photoisomerization results in a large fraction of energy dissipated as heat (up to 90%) on the sub-ns scale, reflecting the low photoisomerization quantum yield (<0.2). This "prompt" step is accompanied by a positive ΔV_1 = 5–12.5 mL mol^{-1}. Formation of the first intermediate is the sole process accessible to PA, with the notable exception of *Slr*1393g3-G for which ΔV_1 = +4.5 mL mol^{-1} is followed by a time-resolved, energy-conserving contraction $\Delta V_2 = -11.4$ mL mol^{-1}, τ_2 = 180 ns at 2.4°C. This peculiarity is possibly due to a larger solvent occupancy of the chromophore cavity for *Slr*1393g3-G.

INTRODUCTION

The details of the initial steps converting photonic energy into chemical energy in energy converters or into molecular movements leading to the signal transduction chain in photosensors are of general interest. In retinal proteins, in photoactive biliproteins and in other photonic signal transducers, the energy stored in the first thermodynamically stable intermediate after primary photochemistry, usually formed on the sub-ns timescale, is of crucial importance: It drives the rest of a photocycle or of a light-induced chain of transient species and depends on several factors, for example structural/conformational changes of chromophore and chromophore cavity, rearrangement of weak interactions and/or steric effects, solvation phenomena following ultrafast charge redistribution or polarization (1,2). Time-resolved photothermal methods have the unique ability to monitor, in real-time, the energy level of transient species and the corresponding volumetric changes of nonthermal origin (ΔV_i) (1). In particular, ns laser photoacoustics (PA) can investigate the sub-ns to short μs time window: Processes occurring faster than ca. 20 ns can be detected as a whole, whereas between 20 ns and maximally ca. 10 μs, PA signals can be resolved in time. For photoactive proteins the fast or "prompt" component (τ_1 < 20 ns) corresponds to formation of the first thermodynamically stable transient species, for example K in bacteriorhodopsin or batho in rhodopsin, while further time-resolved steps correspond to its decay and/or structural rearrangements (2). Combined with optical techniques PA has provided detailed information about the energetics of light-induced early events in many photoreceptors (2). Furthermore, *via* detection of ΔV_i, PA can monitor early light-induced structural or conformational changes, such as fast rearrangements in the hydrogen bond (HB) networks and other weak interactions, that may represent the first stages during signal propagation (3–5). In some cases, it was even possible to correlate the measured ΔV_i, to entropy variations for the K-like transient decay in opsins, thus allowing estimation of free-energy changes for the formation of this intermediate (6,7).

Among the diverse photoreceptors studied by means of photothermal methods (2) phytochromes (phy) and related proteins (8,9) have received relative little attention up to now. Phy are bilin-binding photochromic proteins, where primary photochemistry is the ultrafast (sub-ps) (10) Z → E isomerization of the chromophore C15 = C16 bond, with sub-ns formation of the first thermodynamically stable transient referred to as LUMI (11), where rotation of the tetrapyrrole D-ring has occurred. Plant phy proteins can photoswitch between a Red (R) and a Far Red (FR) state absorbing maximally at ca. 650 and 720 nm (12). A PA study on a plant phytochrome (phyA from *Avena sativa*, *As*phyA) showed that the small isomerization quantum yield (Φ_I = 0.16) for photoswitching from the R to FR forms is reflected in a high fraction of energy released as heat, α = 0.85 on the sub-ns timescale, accompanied by an expansion $\Delta V = \leq +7$ mL mol^{-1} (13). The energy level of the first thermodynamically stable transient, named LUMI-R (or I_{700}), was

*Corresponding author email: aba.losi@fis.unipr.it (Aba Losi)
‡Current address: Department of Biology, South University of Science and Technology of China, Shenzhen, Guangdong, China.
†This article is a part of the Special Issue dedicated to Dr. Wolfgang Gärtner on the occasion of his 65th birthday.

calculated as 150 kJ mol^{-1}, that is LUMI-R stores approximately 84% of the 178 kJ mol^{-1} corresponding to the E_{00} energy. No other transient species were detected, given the limited time window of PA. Further studies with photothermal beam deflection (PBD) that extends into the long μs and ms time-domain showed that two further exothermic expansions occur with lifetimes of 5 and 43 μs, with a large loss of energy that brings the system to an energy level of ca. 18 kJ mol^{-1} (14). It was thus suggested that the subsequent steps toward the final FR state should be driven by entropy rather than enthalpy changes. A major difficulty in dealing with and interpreting PBD data arose from the intrinsic heterogeneity of phy conformational states and the difficulty in choosing between a sequential and a parallel kinetic model for the photocycle (15). These problems are less relevant for PA, due the shorter time window approached and the nature of the detected signal, that is a pressure wave and its time evolution *versus* transient changes in the refraction index for PBD that render separation between heat release and ΔV_i more critical for the latter (1).

Until recently application of PA to phy proteins was of limited interest, given the structural, functional and optical similarities among the various forms of plant phy (8). The situation has drastically changed during the last two decades with the appearance and characterization of many diverse photochromic bilin proteins, mainly from bacteria that show a dramatic spectral versatility, novel physiological functions and that are even good candidates for advanced applications (11). Of particular interest are bilin-binding GAF domains (cGMP-specific phosphodiesterases, cyanobacterial adenylate cyclases and transcription activator FhlA) from cyanobacteriochromes (CBCR). These proteins provide the lyase activity for chromophore binding and are photochromic already as standalone units, different form plant phy and bacteriophytochromes (BphP) (16); in these latter cases, photochromicity requires a PAS-GAF-PHY (PGP) module (Figure 1) (PAS = Per Arnt Sim) (11). In nonphotosynthetic bacteria, BphP uses biliverdin IXα (BV) as chromophore, whereas plants phy and most cyanobacterial phy or CBCR typically utilize the further reduced phytochromobilin (PΦB) and phycocyanobilin (PCB), respectively (8). PΦB and PCB are covalently bound to a cysteine localized within the chromophore-hosting GAF domain, whereas in BphPs, BV is bound to a cysteine in the N-terminal PAS domain, even if the chromophore remains embedded within the GAF domain (11). Spectral versatility and photocycle variability are also major topics for CBCRs and BphPs, with the former spanning the entire UV–vis range (16), and the latter extending the FR form to the near infrared (NIR) spectral region (especially with the so-called Bathy-phytochromes (17)), a very important feature for optogenetics in mammalian cells (18,19). Very recently, CBCRs whose FR form absorbs maximally up to 740 nm have been described, extending the potential of these versatile photoproteins for advanced applications (20). Furthermore, some CBRC-GAF domains are fluorescent with a quantum yield $\Phi_F > 0.05$, a feature of interest for microscopy imaging experiments (21). Notwithstanding their differences, in all phy- and phy-related proteins, the key step during photoconversion is the Z $\rightarrow$ E isomerization of the double C15 = C16 bond during rotation of the D-ring, a process that presumably initiates conformational changes within the chromophore-binding pocket and leads to a signal transduction chain (11,22). All these novel bilin-binding photoreceptors types of prokaryotic origin with their variety of chromophores, protein length, architecture and spectral properties offer a unique opportunity to explore the early energetics of light-triggered reactions and transients and to answer important questions, for example if energy storage in LUMI depends somehow on the parameters listed above and which properties of the cavity dictate the magnitude and sign of the measured ΔV_is.

In this work, we investigated by PA and optical spectroscopy diverse phy and phy-related proteins (Figure 1): (1) the GAF3 (g3) domain of *Synechocystis* CBCR *Slr*1393, a red/green (R/G) photochromic and bi-stable unit (*Slr*1393g3-R and *Slr*1393g3-G) (23); (2) *Synechocystis* Cph1, *Sy*Cph1, exhibiting the familiar red/far red (R/FR) photoconversion pattern (24); (3) full-length and truncated constructs of *Xanthomonas campestris* bacteriophytochrome (*Xcc*BphP, here abbreviated as *Xcp1*), a Bathy-phy with absorbance maxima at 684 nm (*Xcp1*-R) and 758 nm (*Xcp1*-FR) (25–27); the truncated form comprises the PGP module (*Xcp1*PGP); (4) the truncated, 65 kDa form of *Avena sativa* phyA (*As*phyA65) reconstituted with PΦB or PCB (28).

In almost all cases investigated, the formation of LUMI (<20 ns) results in a large fraction of the absorbed energy released as heat (>0.75), reflecting the general low value of Φ_I in this class of photoreceptors. Nevertheless, LUMI stores a large fraction of the E_{00} energy (60–90%), ensuring a major driving force for the progress of light-triggered reactions. Formation of LUMI, in almost all cases the sole step detected by PA, is accompanied by a volume expansion. *Slr*1393g3-G represents a notable exception, in that a large time-resolved, thermally activated and energy-conserving contraction could be detected after the prompt expansion, possibly related to a protein rearrangement involving solvation effects.

MATERIALS AND METHODS

Protein expression and purification. *Xcc*BphP = *Xcp1* (residues 1-634) and the truncated *Xcc*BphP-ΔPAS9 = *Xcp1*PGP (residues 1-511) were amplified from the XC_4241 ORF using *Xanthomonas campestris* pv.

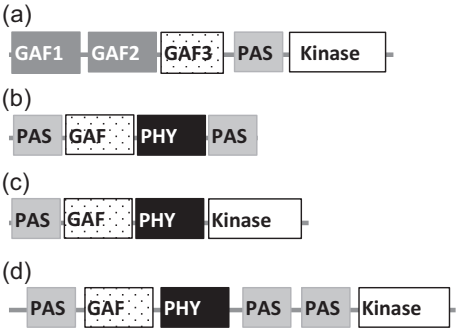

Figure 1. Architecture of proteins or protein domains studied in this work with PA. (a) *Synechocystis Slr*1393 (Uniprot code P73184, 974 aa), a cyanobacteriochrome; *Slr*1393 bear a R/G GAF3 domain binding PCB (*Slr*1393g3, aa 441-597) investigated here; (b) *Xanthomonas campestris* FR/R bacteriophytochrome *Xcp1* (code Q8P3C2, 634 aa), binds BV within the PAS-GAF-PHY (PGP) module; full-length *Xcp1* and *Xcp1*PGP (aa 1-511) were studied in this work; (c) *Synechocystis* Cph1 (code Q55168, 748 aa); and (d) Plant phytochrome *Avena sativa* phyA (code P06593, 1129 aa) are both R/FR phy, binding PCB and PΦB, respectively with a fused Ser/Thr kinase domain (here kinase); for (d) also a truncated PGP version (*As*phyA65, aa 1-595, MW = 65 kDa) was investigated here. GAF domains depicted as gray boxes do not bind bilins, while white, dotted boxes represent chromophore-binding GAF domains. See also text for domain definition.

campestris strain 8004 genomic DNA as by Otero *et al.* (26). Amplicons were cloned into the NdeI/BamHI restriction sites of the pET24A vector (Novagen) to generate pET- ***Xcp1*** and pET- *Xcp1*PGP. *Escherichia coli* BL21(DE3) pLysE cells were transformed with the resulting vectors and cultures induced with a final concentration of 0.4 mM IPTG overnight at 20°C with agitation at 250 rpm. Cells were harvested and ruptured. Next, proteins were purified as previously described (25). Holoproteins were produced by incubation of the apoproteins for 1 h at room temperature in the presence of BV (Sigma-Aldrich) and then subjected to size-exclusion chromatography. *Sy*Cph1 and Slr1393g3 proteins were produced as N-terminal His-tag in *E. coli* BL21(DE3) strain using a pET30 expression vector. All recombinant proteins were expressed by a two-plasmid transformation/expression protocol and purified as previously described (21,29). Briefly, dual plasmid pACYC-ho1-pcyA or pACYC-ho1-hy2 carrying ho1 and pcyA or hy2 that yield PCB or PΦB in *E. coli* for in vivo chromophore assembly. After elution from the Ni-affinity column, imidazole was removed by dialysis against 10 mM potassium phosphate, pH = 7.5. Proteins were then loaded onto a HiPrep DEAE FF 16/10 ion-exchange column (GE Healthcare) to remove most of the unloaded apo-protein if necessary. Recombinant *As*phyA65 was kindly donated by Wolfgang Gaertner and produced as described (28). The final buffers for diluting the proteins were as follows: for *Sy*Cph1 and *Slr*1393g3, 10 mM potassium phosphate, pH = 7.5; for *Xcp1*: 50 mM TRIS, 250 mM NaCl, pH = 7.7; for *As*phyA65: 5 mM potassium phosphate + 2 mM dithiothreitol + 0.2 mM PEFABLOC, pH = 7.6.

Spectroscopic and photoacoustics measurements. Absorption spectra and kinetic traces at single wavelength were recorded with a temperature-controlled Jasco 7850 UV/vis spectrophotometer. Steady-state fluorescence measurements were carried out at 20°C with a Perkin-Elmer LS50 luminescence spectrometer. Formation quantum yields for *Xcp1*-R and *Xcp1*-FR were measured using fluorescence light excitation at 10 nm slit width (650 and 750 nm, respectively) and recording the absorption spectra after defined times of irradiation, as previously described for *Slr*1393g3. As an actinometer for *Xcp1*-R, we used *Slr*1393g3-R for which a value of 0.09 was double-checked with a similar methodology *versus* an absolute method that does not need an actinometer (21). Fluorescence quantum yield for *Xcc*BphP was measured using the reference value of Cph1, Φ_F = 0.024 Cph1-R (30). Photoacoustic (PA) pressure waves were generated by laser pulse absorption from Nd:YAG-driven, tunable OPO laser (Nd:YAG, Innolas, Garching, Germany; OPO, GWU Lasertechnik, Erftstadt, Germany). The following wavelengths of excitation were used: λ_{ex} = 540 nm for *Slr*1393g3-G; λ_{ex} = 630 nm for *Xcp1*-R and *Xcp1*PGP-R; λ_{ex} = 650 nm for *As*phyA-R, *As*phyA65, *Sy*Cph1-R and Slr1393g3-R; λ_{ex} = 660 nm for *Xcp1*-FR and *Xcp1*PGP-FR. PA signals were detected by a PZT piezoelectric transducer (Panametrics V-103). The signal was then amplified (60 db) and recorded by a digitizing oscilloscope (LeCroy 9450A) operated at 2.5 ns per channel. Typically 4000 time points were recorded, within a total time window of 10 μs. The quartz sample cuvette was mounted in a temperature-controlled sample holder (TASC 300, Quantum Northwest, Spokane, WA), which ensured a temperature stability of better than ±0.02°C inside the solution. The beam was shaped by a 1 × 12 mm slit, allowing a time resolution of ~50–60 ns using deconvolution techniques (31). The time window was between 20 ns and 5 μs. Generally, 100 waveforms were averaged for the reference signal, whereas only 16 waveforms were averaged for the samples to avoid extensive photoconversion. Three sets of experiments for each samples were carried out, recording in every instance 2 waveforms at each temperature (for both sample and reference); in this way, we could perform a total of 12 deconvolutions for each temperature and sample. Every four shots, the cuvette was irradiated from above to regenerate the state at the beginning of the experiment with, depending on the case: LEDs (Roithner Lasertechnik GmbH, Vienna, Austria) emitting light of proper maximum wavelength (LED650, LED720, LED760); a CW diode Laser Module emitting at 670 nm with 3mW power (Global Laser, Abertillery, UK); a 532 nm emitting laser pointer (Laserglow Technologies, Toronto, Canada). Data acquisition and analysis were performed using dedicated software (Sound Acquisition and Sound Analysis, Quantum Northwest). The experiments were performed in the linear regime of amplitude *versus* laser fluence, normally ~30 μJ per pulse. New coccine and Brilliant black (FLUKA, Neu-Ulm, Germany) were used as calorimetric references (32). The time evolution of the pressure wave was assumed to be a sum of exponential functions, as previously described (4). The deconvolution analysis yielded the fractional amplitudes (φ_i) and the lifetimes (τ_i) of the transients (Sound Analysis 3000, Quantum Northwest Inc., Spokane, WA). The time window was between 20 ns and 5 μs. At a given temperature and for each resolved *i*-th step, the fractional amplitude φ_i is the sum of the fraction of absorbed energy released as heat (α_i) and the structural volume change *per* absorbed Einstein (ΔV_i), according to Eq. (1) (33):

$$\varphi_i = \alpha_i + \frac{\Delta V_i}{E_\lambda}\frac{c_p\rho}{\beta} \tag{1}$$

where E_λ is the molar excitation energy, $\beta = (\partial V/\partial T)_p \Delta V$ is the volume expansion coefficient, c_p is the heat capacity at constant pressure, and ρ is the mass density of the solvent. In this work, we used the so-called two temperature (TT) method to separate α_i from ΔV_i (34). The sample waveform was acquired at a temperature for which heat transport is zero, $T_{\beta=0}$ (3.9°C in water, exact value depends on the buffer employed) and at a slightly higher temperature $T_{\beta>0}$ = 10°C. At $T_{\beta=0}$, the PA signal of the sample is only due to ΔV_i, whereas the reference signal is zero. The reference for deconvolution was recorded at 10°C, and Eqs. (2a), and (2b) were then used to derive α_i and ΔV_i:

$$\Phi_i \Delta V_i = \varphi_i|_{T_{\beta=0}} \times E_\lambda \left.\frac{\beta}{c_p\rho}\right|_{T_\beta > 0} \tag{2a}$$

$$\alpha_i = \varphi_i|_{T_{\beta>0}} - \varphi_i|_{T_{\beta=0}} \tag{2b}$$

Spectroscopic and PA data were handled and plotted using Origin Professional version 8.5 (Microcal Software, Inc., Northampton, MA, USA).

RESULTS

Fluorescence quantum yields (Φ_F)

In order to obtain information on energy levels of transient species from PA data, it is necessary to estimate Φ_F for each sample (*vide infra*). These values have been already measured for some proteins, that is *Sy*Cph1-R, 0.024 (30); *Slr*1393g3-R, 0.1 and *Slr*1393g3-G, 0.06 (21); *As*phyA, ca. 10^{-3} (35). Comparing *Xcp1*-R with *Sy*Cph1 gave a comparable value of 0.022, whereas in *Xcp1*-FR fluorescence appears negligible (Figure 2).

Photoacoustic measurements

With the exception of *Slr*1393g3-G, PA signals from the investigated proteins were best analyzed with a single exponential function, with an unresolved component τ_1 < 20 ns (Table 1). This finding is very similar to the behavior reported for full-length *As*phyA-R (13) and corresponds to formation of LUMI (also called I_{700} in *As*phyA-R) that follows chromophore isomerization and D-ring rotation. Formation of LUMI invariably corresponds to a volume expansion (Table 1, Figure 3).

Energy balance considerations and the results of deconvolution directly provide the product $\Phi_1 E_1$ (Eq. 3), where it should hold $\Phi_1 = \Phi_I$ and E_1 = energy level of LUMI:

$$\Phi_1 \frac{E_1}{E_\lambda} = 1 - \alpha_1 - \Phi_F \frac{E_F}{E_\lambda} \tag{3}$$

Here, E_F is the average energy for the fluorescence emission and E_λ is the photonic energy corresponding to λ_{ex}. It is clear that E_λ is an upper value for E_1; therefore, it is straightforward from Eq. (3) to estimate a lower limit for Φ_I, once the fluorescence parameters are known. If fluorescence is measurable and the 0-0 energy level (E_{00}) can be established, this latter value can be taken instead of E_λ as an upper limit for E_1.

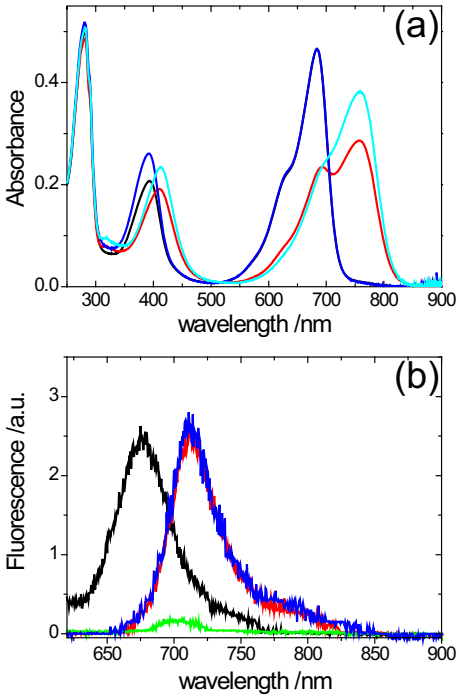

Figure 2. (a) Absorption spectra of *Xcp1* and *Xcp1*PGP in the R form (black and blue lines) and in the dark adapted state (red and cyan line, respectively). Assuming that *Xcp1*PGP in the dark is 100% in the FR form, the full-length protein in the same condition can be estimated to an equilibrium between R (15%) and FR (85%, simulation is not shown). (b) Fluorescence spectra of Cph1-R (Φ_F = 0.024, black), *Xcp1*-R (blue) and *Xcp1*PGP-R (red). λ_{ex} was at 580 nm, 20°C. FR forms have negligible fluorescence, originating from residual *Xcp1*-R (green line for *Xcp1*PGP-FR). Integrating the areas gave Φ_F = 0.022 for both *Xcp1*-R and *Xcp1*PGP-R.

Neither truncation at the photosensing module level nor chromophore substitution affect PA parameters in *As*phya65-R (Table 1). The smaller $\Phi_1\Delta V_1$ recorded for the R forms of *Sy*Cph1 and *Slr*1393g3 is thus not related to PCB, but is intrinsic to these proteins. Spectral separation and FR form accumulation were not sufficient to carry out PA experiments with *As*phya65-FR and *Sy*Cph1-FR. Conditions are more favorable with *Sy*Cph1 and *Slr*1393g3 and *Xcp1*. *Slr*1393g3-G can in fact be accumulated with 670 nm irradiation and photo-excited with green light, whereas *Xcp1*PGP-FR is the dark adapted state of truncated *Xcp1*(26). In the dark, full-length *Xcp1* is in equilibrium (Figure 2) containing 85% FR form under our conditions. After an experiment, we measured a total photoconversion to the R form of only 5%; therefore, the data appear to be reliable. We tentatively excited *Xcp1*-FR with 660 nm light, as in the NIR range no suitable calorimetric reference compound was at hand for aqueous solutions. Also for the FR forms we measured a "prompt" expansion $\Phi_1\Delta V_1$, somewhat larger than for the R forms. In *Slr*1393g3-G the value of $\Phi_1\Delta V_1$ is instead sixfold larger than in *Slr*1393g3-R.

Table 2 summarizes the values for Φ_I as determined by optical methods and the derived ΔV_1 and E_1. A discrepancy can be seen for *Slr*1393g3-R and *Sy*Cph1-R for which Φ_I would give an energy level for LUMI larger than the excitation energy. It must be noted that it is normally assumed that the quantum yield of a photocycle, or in a chain of light-triggered reactions, is the same as the quantum yield for the primary photochemical reaction, that is no dissipative steps are considered, which might not be always the case. Although errors associated with quantum yields are generally large, here the difference is quite large and points to dissipative processes outside our time window for these two protein forms. Another possibility is the existence of different chromophore geometries ("active" and "silent") with very different Φ_I and the fraction of each form depending on temperature, a kind of heterogeneity up to now established and investigated for *Slr*1393g3-R (36), but not *Sy*Cph1-R.

As for *Xcp1* proteins it is clear that, similar to *As*phyA, truncation does not lead to appreciable differences in the PA parameters. Results from *Xcp1* and *Slr*1393g3 also underscore that Z/E isomerization leads to a fast volume expansion, independently of the isomerization direction.

*Slr*1393g3-G behaves different from all other proteins, in that the fast expansion is followed by a contraction, with virtually no further release of heat (Figure 3, Table 3).

This negative ΔV_2 corresponds to the decay of the primary thermodynamically stable photoproduct into the next state of the phototransformation and has an associated lifetime τ_2 = 180 ns at 2.4°. τ_2 for this transition shows a sharp temperature dependence leading to a straight Arrhenius plot (Figure 4) that provides an activation energy E_a = 38 kJ mol^{-1}. The low value of the pre-exponential factor, A = 109000 s^{-1}, indicates that the activation entropy is negative, that is unfavorable, indeed the Eyring plot (not shown) gave an activation entropy change $\Delta S^{\#} = -0.15$ kJ mol^{-1} K^{-1} and an activation enthalpic variation $\Delta H^{\#}$ = 36 kJ mol^{-1}.

Table 1. Photoacoustics parameters measured for the "prompt" step (below 20 ns, isomerization).

Protein	λ_{ex}/nm (E_λ, kJ mol^{-1})	α_1	$\Phi_1\Delta V_1$ (mL mol^{-1})	Φ_1 E_1 (kJ mol^{-1})	Φ_1	E_{00} (kJ mol^{-1})
*As*phyA-R*	650 (180.0)	0.88 ± 0.04	0.92 ± 0.23	21.6 ± 7.2	≥0.13	178
*As*phyA65-R -PΦB	650 (180.0)	0.88 ± 0.04	0.90 ± 0.06	21.6 ± 7.2	≥0.12	178
*As*phyA65-R- PCB	650 (180.0)	0.88 ± 0.05	0.75 ± 0.06	21.6 ± 9.0	≥0.12	178
Xcp1-R	630 (189.9)	0.89 ± 0.02	1.34 ± 0.05	17.2 ± 3.8	≥0.10	171
*Xcp1*PGP-R	630 (189.9)	0.92 ± 0.02	1.08 ± 0.05	11.3 ± 4.2	≥0.07	171
Xcp1-FR	660 (181.2)	0.92 ± 0.03	1.28 ± 0.04	14.5 ± 5.4	≥0.08†	n.d.†
*Xcp1*PGP-FR	660 (181.2)	0.92 ± 0.03	1.50 ± 0.09	14.5 ± 5.4	≥0.08†	n.d.†
*Sy*Cph1-R	650 (180.0)	0.79 ± 0.02	0.22 ± 0.05	34.4 ± 3.7	≥0.19	180.4
*Slr*1393g3-R	650 (180.0)	0.76 ± 0.02	0.21 ± 0.03	26.6 ± 3.7	≥0.15	180.4
*Slr*1393g3-G	540 (221.5)	0.71 ± 0.03	1.36 ± 0.07	52.8 ± 6.6	≥0.26	202.7

*We took the average values upon 650 nm exc. in (13). †Given that E_{00} is unknown, for lack of fluorescence, the value of E_λ as upper level for E_1 was used. Given errors for the PA parameters, originate from three separate experiments for each sample, as detailed in Materials and Methods.

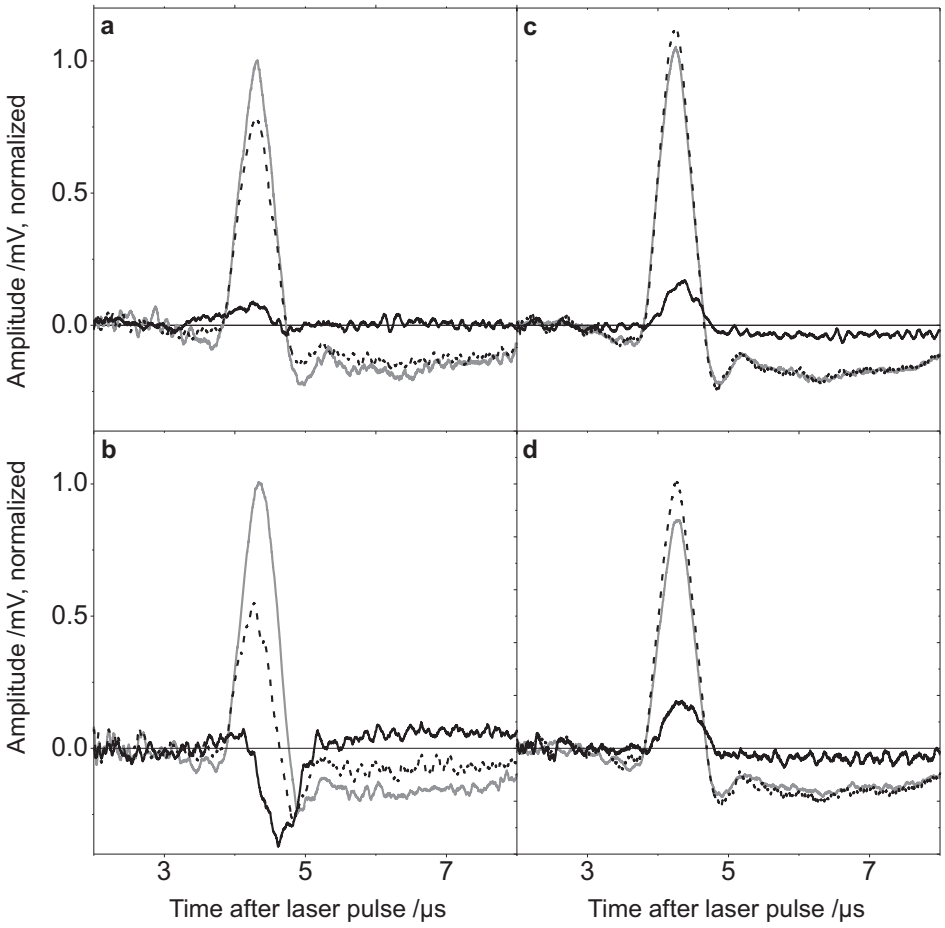

Figure 3. Photoacoustics signals at $T_{\beta > 0}$ = 10°C for the reference compound (gray lines) and selected proteins (dotted lines); the full black lines represent the signal from proteins at $T_{\beta = 0}$ (varies with the buffer), where the reference compound has zero amplitude (not shown). (a) *Slr*1393g3-R, $T_{\beta = 0}$ = 2.4°C; (b) *Slr*1393g3-G, $T_{\beta = 0}$ = 2.4°C; (c) *Xcp1*PGP-R, $T_{\beta = 0}$ = −1.5°C; (d) *Xcp1*PGP-FR, $T_{\beta = 0}$ = −1.5°C. Note the sharp contraction for *Slr*1393g3-G, following a very small expansion (see Tables 1 and 2).

DISCUSSION

In phy and phy-related proteins, chromophore Z/E isomerization produces a fast (τ_1 < 20 ns) volume expansion, irrespective of whether it occurs in the Z → E or E → Z direction. This is in line with PA data on opsin photosensors, for which isomerization invariably produces a prompt ΔV_1 = +5.0 to +10 mL mol^{-1} (2) for formation of the K-like intermediate. The range of ΔV_1 measured in this work for phy-related proteins, +4.5 to + 12.5 mL mol^{-1} (Table 1), is fully in line with the data determined for the opsins. Given that on this time scale volume changes mainly reflect weak interactions modifications and steric rearrangements after primary photochemistry, a $\Delta V_1 > 0$ in phy- and opsin proteins points to a prevalence of the latter factor, that is photoisomerization seems to require an enlargement of the cavity in order to accommodate the new chromophore geometry, in case of the phy proteins due to D-ring reorientation during isomerization of the C15 = C16 bond. A notable exception is photoactive yellow protein (PYP), where instead fast HB strengthening around the isomerized chromophore produces a contraction, ΔV_1 = −14 mL mol^{-1} (37). This becomes apparent from studies of the E46A mutation of PYP: The disruption of the HB network now shifts ΔV_1 to + 6 mL mol^{-1} (3). In the phy and opsin proteins, isomerization produces similar effects, strengthening the hypothesis that $\Delta V_1 > 0$ reflects mainly steric and geometric rearrangements. Recently, quantum mechanics/molecular mechanics calculations on *Deinococcus radiodurans* BphP (*Dr*BphP) have shown that steric effects are indeed a key factor in determining isomerization selectivity and efficiency, when the bilin chromophore is embedded within the protein (38). In

Table 2. Spectroscopically measured quantum yields and LIOAS-derived parameters for the "prompt" step (τ_1 < 20 ns, isomerization).

Protein	Φ_I	E_1 (kJ mol^{-1})	ΔV_1 (mL mol^{-1})	E_1/E_{00}
*As*phyA-R	0.16	135 ± 45	5.7 ± 1.4	0.76
*As*phyA65-R -PΦB	0.16	135 ± 45	5.6 ± 0.4	0.76
*As*phyA65-R- PCB	0.16	135 ± 56	4.7 ± 0.4	0.76
Xcp1-R	0.15	115 ± 25	8.9 ± 0.3	0.67
*Xcp1*PGP-R	0.12	94 ± 35	9.0 ± 0.4	0.55
Xcp1-FR	0.15	97 ± 36	10 ± 0.3[†]	n.d.*
*Xcp1*PGP-FR	0.12	121 ± 45	12.5 ± 0.7	n.d.*
*Sy*Cph1	0.15[‡]	≤180.4	≤1.1 ± 0.3	n.d.[‡]
*Slr*1393g3-R	0.09[‡]	≤180.4	≤1.4 ± 0.2	n.d.[‡]
*Slr*1393g3-G	0.3	176 ± 22	4.5 ± 0.2	0.87

*E_{00} cannot be determined, for lack of fluorescence. [†]It is taken into account that full-length *Xcp1* is only 85% in the FR form. [‡]These values of Φ_I would give $E_1 > E_\lambda$. See text for details.

Table 3. Photoacoustics-derived parameters for *Slr*1393g3-G.

Protein	Φ_1	E_1 (kJ mol^{-1})	ΔV_1 (mL mol^{-1})	E_2 (kJ mol^{-1})	ΔV_2 (mL mol^{-1})	τ_2/ns ($T_{\beta\,=\,0}$ = 2.4°C)
*Slr*1393g3-G	0.3	176 ± 22	4.5 ± 0.2	164 ± 25	−11.4 ± 0.2	180 ± 10

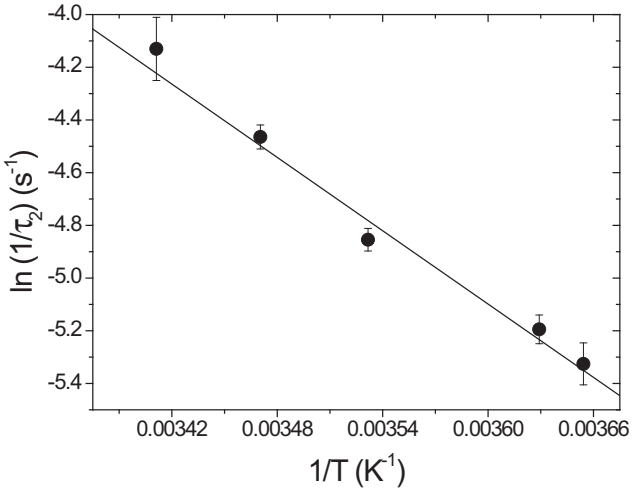

Figure 4. Arrhenius plot for the second, time-resolved component of PA signals for *Slr*1393g3-G. Measured τ_2 ranges from 206 ± 16 ns (0.5°C) to 62 ± 8 ns (20°C). Given errors originate from three separate experiments, as detailed in Materials and Methods.

*Sy*Cph1-R, two different D-ring geometries exists, one of which is thought to be planar (silent) and the second has a pretwisted C15 = C16 double bond induced by HB to H290 (active); as a consequence of pretwisting, the latter has a much higher Φ_I = 0.29 (*vs* 0.03 for the former) (36). On the other hand, mutations that hinder or block D-ring reorientation *via* additional weak interactions or bulky residues are expected to have a lower Φ_I, a feature that has been several times verified underscoring the relevance of geometric factors (36).

The "prompt" expansion measured with PA is much smaller for *Sy*Cph1-R and *Slr*1393g3-R than in *As*phyA and *Xcp1*. Inspection of the cavity, in terms of residues surrounding the chromophore in available 3D structures (Figure 5), does not offer hints about the reasons for this difference. Packing of amino acid side chains around ring D appears to be in all cases relatively loose, as previously noticed for *Deinococcus radiodurans* BphP (*Dr*BphP) (39) carrying BV as chromophore. The smaller expansion in *Sy*Cph1-R and *Slr*1393g3-R could be considered to be due to the different chromophore (BV *vs* PCB), but this is ruled out by the negligible effects of PΦB substitution with PCB in *As*phyA (Table 1). Another factor affecting ΔV_1 could be water occupancy in the vicinity of the chromophore. In the crystallographic structure of *An*PixJg2-R, a R/G photoswitching GAF domain with strong similarity to *Slr*1393g3, a pyrrole water is missing and the conserved aspartic acid makes direct HB contact directly with ring B and C N–H groups (40). In canonic phy, the pyrrole water molecule participates instead in the HB network, but this is the case also in *Sy*Cph1-R (39,41,42), therefore also this factor can be ruled out and the reasons for the smaller ΔV_1 in these two cases remains elusive.

Thanks to the several constructs employed in this work, we are able to conclude that the "prompt" expansion ΔV_1 certainly reflects structural changes that on this short timescale remain

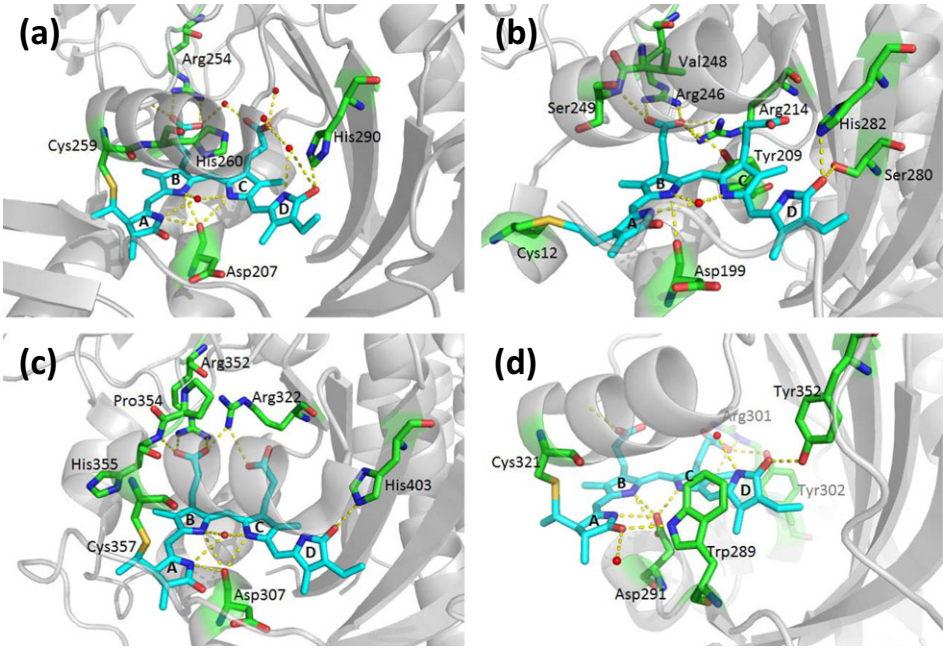

Figure 5. Insights into the chromophore-binding GAF domain of selected phy-related proteins, in the dark adapted state. Ring D is adjacent to the C15 = C16 double bond undergoing isomerization. Protein Data Bank accession codes are given in parenthesis. (a) *Sy*Cph1-R (2VEA); (b) *Xcp1*, mostly in FR form (5AKP); (c) *Arabidopsis thaliana* phyB-R (4OUR); (d) *An*PixJg2-R (3W2Z). Figures were generated using Pymol (45).

confined to the vicinity of the chromophore. In fact, truncation leaving only the PGP module has no effects on ΔV_1 (see Tables 1 and 2). Also, there is no remarkable difference between *Sy*Cph1-R (a full-length protein) and *Srl*1393g3-R, a single GAF domain. This concept is in line with recent results obtained by time-resolved X-ray scattering and Fourier transform infrared spectroscopy (FTIR experiments) on various constructs of *Dr*BphP: Structural changes up to the microsecond timescales are small and appear to be localized within the chromophore-binding domain, while large-scale movements and conformational changes occur in the ms time window (43,44).

An important aspect obtained from this study is the result that a high percentage of the excitation energy is stored in LUMI, between 55 and 87% of E_{00}, underscoring the protein strain and the low entropic gain at this early timescale (<20 ns), as already noticed for other sensory photoreceptors (2). The highest value was measured for *Slr*1393g3-G, a protein form that also shows another peculiarity, that is an energy conserving, temperature activated and quite large volume contraction on the tens ns timescale: This step is undetected in flash photolysis experiments (23) and may correspond to an optically silent transition involving water molecules. It has been demonstrated that in the similar *An*PixJg2 protein, a tryptophan acts as a water gate and solvent occupation becomes larger in the G-form (40). The gate mechanism is considered to be a major determinant for color tuning in these proteins, and this Trp is conserved also in *Slr*1393g3. Given that ΔV_2 has a temperature activated kinetics, it is conceivable that this contraction reflects water rearrangements/ingress within the chromophore pocket, immediately after chromophore isomerization.

CONCLUSIONS

The large availability of bilin-binding, phy-related proteins of different origin and with diverse characteristics, allows nowadays the application of photothermal methods to unravel the time-resolved energetics in the early photochemical processes of these widespread photoreceptors. We have shown here that LUMI invariably stores a large percentage of the excitation energy, thus ensuring the thermodynamic driving force for progression of light-initiated reactions. Isomerization results in a volume expansion, independent of its direction, underscoring the relevance of steric/geometric effects. In this work, we also highlighted the peculiar behavior of a red/green photochromic GAF domain from a CBRC protein and detected an optically silent transition possibly involving the rearrangement of water molecules in *Slr*1393g3-G.

Acknowledgements—We thank Wolfgang Gärtner for samples of purified *As*phyA. K.T. is supported by the National Natural Science Foundation of China (Grant 31600612) and a doctoral fellowship from the China Scholar Council.

REFERENCES

1. Gensch, T. and C. Viappiani (2003) Time-resolved photothermal methods: Accessing time-resolved thermodynamics of photoinduced processes in chemistry and biology. *Photochem. Photobiol. Sci.* **2**, 699–721.
2. Losi, A. and S. E. Braslavsky (2003) The time-resolved thermodynamics of the chromophore-protein interactions in biological photosensors. Learning from photothermal measurements. *Phys. Chem. Chem. Phys.* **5**, 2739–2750.
3. Losi, A., T. Gensch, M. A. van der Horst, K. J. Hellingwerf and S. E. Braslavsky (2005) Hydrogen-bond network probed by time-resolved optoacoustic spectroscopy: The case of photoactive yellow protein and the effect of E46Q and E46A mutations. *Phys. Chem. Chem. Phys.* **7**, 2229–2236.
4. Raffelberg, S., M. Mansurova, W. Gärtner and A. Losi (2011) Modulation of the photocycle of a LOV domain photoreceptor by the hydrogen bonding network. *J. Am. Chem. Soc.* **133**, 5346–5356.
5. Raffelberg, S., A. Gutt, W. Gärtner, C. Mandalari, S. Abbruzzetti, C. Viappiani and A. Losi (2013) The amino acids surrounding the flavin 7a-methyl group determine the UVA spectral features of a LOV protein. *Biol. Chem.* **394**, 1517–1528.
6. Losi, A., A. A. Wegener, M. Engelhardt and S. E. Braslavsky (2001) Enthalpy-entropy compensation in a photocycle: The K to L transition in sensory rhodopsin II from *Natronobacterium pharaonis*. *J. Am. Chem. Soc.* **123**, 1766–1767.
7. Losi, A., A. A. Wegener, M. Engelhard and S. E. Braslavsky (2001) Thermodynamics of the early steps in the photocycle of *Natronobacterium pharaonis* halorhodopsin. influence of medium and of anion substitution. *Photochem. Photobiol.* **74**, 495–503.
8. Rockwell, N. C., Y. S. Su and J. C. Lagarias (2006) Phytochrome structure and signaling mechanisms. *Annu. Rev. Plant Biol.* **57**, 837–858.
9. Nagano, S. (2016) From photon to signal in phytochromes: similarities and differences between prokaryotic and plant phytochromes. *J. Plant. Res.* **129**, 123–135.
10. Dasgupta, J., R. R. Frontiera, K. C. Taylor, J. C. Lagarias and R. A. Mathies (2009) Ultrafast excited-state isomerization in phytochrome revealed by femtosecond stimulated Raman spectroscopy. *Proc. Natl Acad. Sci. USA* **106**, 1784–1789.
11. Anders, K. and L. O. Essen (2015) The family of phytochrome-like photoreceptors: diverse, complex and multi-colored, but very useful. *Curr. Opin. Struct. Biol.* **35**, 7–16.
12. Li, J., G. Li, H. Wang and X. Wang Deng (2011) Phytochrome signaling mechanisms. *Arabidopsis Book/Am. Soc. Plant. Biol.* **9**, e0148.
13. Gensch, T., M. S. Churio, S. E. Braslavsky and K. Schaffner (1996) Primary quantum yield and volume change of phytochrome-A phototransformation determined by Laser-Induced Optoacoustic Spectroscopy. *Photochem. Photobiol.* **63**, 719–725.
14. Michler, I. and S. E. Braslavsky (2001) Time-resolved thermodynamic analysis of the oat phytochrome A phototransformation. A photothermal beam deflection study. *Photochem. Photobiol.* **74**, 624–635.
15. Schmidt, P., T. Gensch, A. Remberg, W. Gärtner, S. E. Braslavsky and K. Schaffner (1998) The complexity of the Pr to Pfr phototransformation kinetics is an intrinsic property of native phytochrome. *Photochem. Photobiol.* **68**, 754–761.
16. Bhaya, D. (2016) In the limelight photoreceptors in cyanobacteria. *MBio* **7**, e00741-16.
17. Rottwinkel, G., I. Oberpichler and T. Lamparter (2010) Bathy phytochromes in rhizobial soil bacteria. *J. Bacteriol.* **192**, 5124–5133.
18. Shcherbakova, D. M., A. A. Shemetov, A. A. Kaberniuk and V. V. Verkhusha (2015) Natural photoreceptors as a source of fluorescent proteins, biosensors, and optogenetic tools. *Annu. Rev. Biochem.* **84**, 519–550.
19. Kaberniuk, A. A., A. A. Shemetov and V. V. Verkhusha (2016) A bacterial phytochrome-based optogenetic system controllable with near-infrared light. *Nat. Meth.* **13**, 591–597.
20. Rockwell, N. C., S. S. Martin and J. C. Lagarias (2016) Identification of cyanobacteriochromes detecting far-red Light. *Biochemistry* **55**, 3907–3919.
21. Pennacchietti, F., A. Losi, X. L. Xu, K. H. Zhao, W. Gärtner, C. Viappiani, F. Cella, A. Diaspro and S. Abbruzzetti (2015) Photochromic conversion in a red/green cyanobacteriochrome from *Synechocystis* PCC6803: quantum yields in solution and photoswitching dynamics in living *E. coli* cells. *Photochem. Photobiol. Sci.* **14**, 229–237.
22. von Horsten, S., S. Strass, N. Hellwig, V. Gruth, R. Klasen, A. Mielcarek, U. Linne, N. Morgner and L. O. Essen (2016) Mapping light-driven conformational changes within the photosensory module of plant phytochrome B. *Sci. Rep.* **6**, 34366.
23. Xu, X. l., A. Gutt, J. Mechelke, S. Raffelberg, K. Tang, D. Miao, L. Valle, C. D. Borsarelli, K. H. Zhao and W. Gärtner (2014)

Combined mutagenesis and kinetics characterization of the bilin-binding GAF domain of the protein *Slr*1393 from the cyanobacterium *Synechocystis* PCC6803. *ChemBioChem* **15**, 1190–1199.
24. Lamparter, T., F. Mittmann, W. Gartner, T. Borner, E. Hartmann and J. Hughes (1997) Characterization of recombinant phytochrome from the cyanobacterium *Synechocystis*. *Proc. Nat. Acad. Sci. USA* **94**, 11792–11797.
25. Klinke, S., L. H. Otero, J. Rinaldi, S. Sosa, B. G. Guimar+úes, W. E. Shepard, F. A. Goldbaum and H. R. Bonomi (2014) Crystallization and preliminary X-ray characterization of the full-length bacteriophytochrome from the plant pathogen *Xanthomonas campestris* pv. *campestris*. *Acta Crystallogr. Sect. F Struct. Biol. Cryst. Commun.* **70**, 1636–1639.
26. Otero, L. H., S. Klinke, J. Rinaldi, F. Velázquez-Escobar, M. A. Mroginski, M. Fernández -López, F. Malamud, A. A. Vojnov, P. Hildebrandt, F. A. Goldbaum and H. R. Bonomi (2016) Structure of the full-length bacteriophytochrome from the plant pathogen *Xanthomonas campestris* provides clues to its long-range signaling mechanism. *J. Mol. Biol.* **19**, 3702–3720.
27. Bonomi, H. R., L. Toum, G. Sycz, R. Sieira, A. M. Toscani, G. E. Gudesblat, F. C. Leskow, F. A. Goldbaum, A. A. Vojnov and F. Malamud (2016) *Xanthomonas campestris* attenuates virulence by sensing light through a bacteriophytochrome photoreceptor. *EMBO Rep.* **17**, 1565–1577.
28. Mozley, D., A. Remberg and W. Gartner (1997) Large-scale generation of affinity-purified recombinant phytochrome chromopeptide. *Photochem. Photobiol.* **66**, 710–715.
29. Zhang, J., X. J. Wu, Z. B. Wang, Y. Chen, X. Wang, M. Zhou, H. Scheer and K. H. Zhao (2010) Fused-gene approach to photoswitchable and fluorescent Biliproteins. *Angew. Chem. Int. Ed.* **49**, 5456–5458.
30. Mailliet, J., G. Psakis, K. Feilke, V. Sineshchekov, L. O. Essen and J. Hughes (2011) Spectroscopy and a high-resolution crystal structure of Tyr263 mutants of cyanobacterial phytochrome Cph1. *J. Mol. Biol.* **413**, 115–127.
31. Rudzki, J. E., J. L. Goodman and K. S. Peters (1985) Simultaneous determination of photoreaction dynamics and energetics using pulsed, time resolved photoacoustic calorimetry. *J. Am. Chem. Soc.* **107**, 7849–7854.
32. Abbruzzetti, S., C. Viappiani, D. H. Murgida, R. Erra-Balsells and G. M. Bilmes (1999) Non-toxic, water-soluble photocalorimetric reference compounds for UV and visible excitation. *Chem. Phys. Lett.* **304**, 167–172.
33. Rudzki-Small, J., L. J. Libertini and E. W. Small (1992) Analysis of photoacoustic waveforms using the nonlinear least square method. *Biophys. Chem.* **41**, 29–48.
34. Malkin, S., M. S. Churio, S. Shochat and S. E. Braslavsky (1994) Photochemical energy storage and volume changes in the microsecond time range in bacterial photosynthesis – a laser induced optoacoustic study. *J. Photochem. Photobiol. B: Biol.* **23**, 79–85.
35. Colombano, C. G., S. E. Braslavsky, A. R. Holzwarth and K. Schaffner (1990) Fluorescence quantum yields of 124-kDa phytochrome from oat upon excitation with different absorption bands. *Photochem. Photobiol.* **52**, 19–22.
36. Yang, Y., M. Linke, T. von Haimberger, R. Matute, P. Schmieder and K. Heyne (2014) Active and silent chromophore isoforms for phytochrome Pr photoisomerization: An alternative evolutionary strategy to optimize photoreaction quantum yields. *Struct. Dyn.* **1**, 014701.
37. Brederode, M. E. V., T. Gensch, W. D. Hoff, K. J. Hellingwerf and S. E. Braslavsky (1995) Photoinduced volume change and energy storage associated with the early transformations of the photoactive yellow protein from *Ectothiorhodospira halophila*. *Biophys. J.* **68**, 1101–1109.
38. Falklöf, O. and B. Durbeej (2016) Steric effects govern the photoactivation of phytochromes. *Chem. Phys. Chem.* **17**, 954–957.
39. Wagner, J. R., J. S. Brunzelle, K. T. Forest and R. D. Vierstra (2005) A light-sensing knot revealed by the structure of the chromophore-binding domain of phytochrome. *Nature* **438**, 325–331.
40. Velazquez Escobar, F., T. Utesch, R. Narikawa, M. Ikeuchi, M. A. Mroginski, W. Gärtner and P. Hildebrandt (2013) Photoconversion mechanism of the second GAF domain of cyanobacteriochrome *An*PixJ and the cofactor structure of its green-absorbing state. *Biochemistry* **52**, 4871–4880.
41. Essen, L. O., J. Mailliet and J. Hughes (2008) The structure of a complete phytochrome sensory module in the Pr ground state. *Proc. Natl Acad. Sci. USA* **105**, 14709–14714.
42. Burgie, E. S., A. N. Bussell, J. M. Walker, K. Dubiel and R. D. Vierstra (2014) Crystal structure of the photosensing module from a red/far-red light-absorbing plant phytochrome. *Proc. Natl Acad. Sci. USA* **111**, 10179–10184.
43. Björling, A., O. Berntsson, H. Lehtivuori, H. Takala, A. J. Hughes, M. Panman, M. Hoernke, S. Niebling, L. Henry, R. Henning, I. Kosheleva, V. Chukharev, N. V. Tkachenko, A. Menzel, G. Newby, D. Khakhulin, M. Wulff, J. A. Ihalainen and S. Westenhoff (2016) Structural photoactivation of a full-length bacterial phytochrome. *Sci. Adv.* **2**, e1600920.
44. Takala, H., S. Niebling, O. Berntsson, A. Björling, H. Lehtivuori, H. Häkkänen, M. Panman, E. Gustavsson, M. Hoernke, G. Newby, F. Zontone, M. Wulff, A. Menzel, J. A. Ihalainen and S. Westenhoff (2016) Light-induced structural changes in a monomeric bacteriophytochrome. *Struct. Dyn.* **3**, 054701.
45. DeLano, W. L. (2002) PyMOL: An open-source molecular graphics tool. *Newslett. Protein Crystallograp.* **40**, 82–92.